ELSEVIER

Journal of Alloys and Compounds 416 (2006) 284–290

Journal of ALLOYS AND COMPOUNDS

www.elsevier.com/locate/jallcom

Influence of ruthenium ions on the precipitation of α-FeOOH, α-Fe_2O_3 and Fe_3O_4 in highly alkaline media

Stjepko Krehula, Svetozar Musić *

Division of Materials Chemistry, Ruđer Bošković Institute, P.O. Box 180, HR-10002 Zagreb, Croatia

Received 13 August 2005; accepted 1 September 2005
Available online 27 October 2005

Abstract

The influence of ruthenium ions on the precipitation of goethite (α-FeOOH), α-Fe_2O_3 and Fe_3O_4 in highly alkaline media was investigated by ^{57}Fe Mössbauer and FT-IR spectroscopies, thermal field emission scanning electron microscope (FE SEM) and EDS. The presence of Ru-dopant strongly affected the precipitation of α-FeOOH at highly alkaline pH, i.e. the formation of α-Fe_2O_3 was also noticed. A decrease of hyperfine magnetic field (HMF) at RT from 35.1 T (undoped α-FeOOH) to 31.3 T for sample with [Ru]/([Ru] + [Fe]) = 0.0196 was assigned to the incorporation of ruthenium ions into the α-FeOOH structure. Mössbauer spectroscopy showed the formation of stoichiometric Fe_3O_4 for [Ru]/([Ru] + [Fe]) = 0.0291–0.0909. α-Fe_2O_3 and Fe_3O_4 did not show a tendency to the formation of solid solutions with ruthenium ions. FE SEM observations of the samples showed that reference α-FeOOH sample contained acicular particles of good uniformity, which increased the length up to ∼5 times with increase of concentration of ruthenium ions. On the other hand, large octahedral Fe_3O_4 crystals (particles) were associated with small particles of ruthenium (hydrous) oxide with a size in the range ∼100 nm or less. A possible catalytic action of ruthenium that created reduction conditions for Fe^{3+} ions and formation of Fe^{2+} ions for precipitation of Fe_3O_4 was discussed.

Keywords: Ru-dopant; Tetramethylammonium hydroxide; α-FeOOH; α-Fe_2O_3; Fe_3O_4; ^{57}Fe Mössbauer; FT-IR; FE SEM; EDS

1. Introduction

Goethite (α-FeOOH) is naturally present in various soils, marine sediments and ore deposits. As a rule, natural α-FeOOH is not pure, and it may contain metal cations substituted in various concentrations. α-FeOOH is a dominant fraction in limonite ore ($FeOOH{\cdot}nH_2O$) which is used in the production of iron. Also, α-FeOOH is the constituent of the rust formed by atmospheric or "wet" corrosion of iron (steel). The fraction of α-FeOOH phase in the rust depends on the conditions of the rusting of iron (steel). The color of natural α-FeOOH can vary from lemon yellow to dark brown, and the changes in the color are not only due to the particle size differences, but are also a consequence of the metal cation substitutions.

Synthetic α-FeOOH can be prepared in a chemical laboratory by: (a) hydrolysis of $Fe(NO_3)_3$ aqueous solutions at low pH values, (b) precipitation from Fe(III)–salt solutions at a very high pH and (c) oxidation of $Fe(OH)_2$ suspensions with air or O_2. Synthetic α-FeOOH in the form of acicular α-FeOOH particles is used as a starting material in the production of acicular maghemite (γ-Fe_2O_3) particles via magnetite (Fe_3O_4) as a transition phase. The acicular shape of the particles could be preserved during all stages of this synthesis. The researchers made a significant effort in the investigation of the metal cation substitutions in iron(III)-oxyhydroxides and -oxides due to their importance in the industry and environment.

Cadmium ions in an aqueous environment are very toxic for humans, and they come from mines or various industrial wastes. Cd^{2+} ions can be removed from contaminated aqueous solutions by α-FeOOH using an adsorption/coprecipitation mechanism. Cd^{2+} ions can be incorporated up to ∼9.5% of the Fe^{3+} ions in the octahedra of α-FeOOH [1]. A progressive increase in the size of the unit-cell parameters and unit-cell volume of α-FeOOH due to the much larger Cd^{2+} ion (0.95 Å) compared with Fe^{3+} (0.645 Å) was noticed, as well as a decrease of crystallinity. Sileo et al. [2] monitored incorporation of Cd^{2+} ions in α-FeOOH in alkaline media. The authors noticed a drastic decrease of incorporation of Cd^{2+} into α-FeOOH structure for $\mu_{cd} = 7.03$

* Corresponding author.
E-mail address: music@irb.hr (S. Musić).

0925-8388/$ – see front matter © 2005 Elsevier B.V. All rights reserved.
doi:10.1016/j.jallcom.2005.09.016

expressed as $\mu_{cd} = 100 \times [Cd]/\{[Cd] + [Fe]\}$, whereas a probable formation of Cd-substituted hematite (α-Fe_2O_3) was suggested. Singh et al. [3] used an Extended X-Ray Absorption Fine Structure (EXAFS) spectroscopy to investigate incorporation of Cr^{3+}, Mn^{2+} and Ni^{2+} into the α-FeOOH structure, and the authors found that up to 8 mol% Cr, 15 mol% Mn and 5 mol% Ni can be incorporated. Stiers and Schwertmann [4] also found that up to 15 mol% Mn can be incorporated into the synthetic α-FeOOH. On the basis of the unit-cell measurements, the authors concluded about oxidation to Mn^{3+} for Mn-substituted goethite. Vandenberghe et al. [5] investigated Mn-substituted α-$(Fe_{1-c}Mn_c)OOH$ and α-$(Fe_{1-c}Mn_c)_2O_3$ with c up to 0.08. The hyperfine magnetic field was less influenced by Mn substitution than with Al. However, Mn substitution drastically suppressed the Morin transition in α-Fe_2O_3 which resulted in a weakly ferromagnetic state at 80 K for $c > 0.04$. Natural α-FeOOH samples from the oxidized level of the Vermelho Ni-lateritic deposit (Brazilian Amazonia) were investigated by Mössbauer spectroscopy and other techniques [6]. Natural Ni-containing α-FeOOH did not incorporate more than ~4 mol% Ni. Also, this mineral contained significant amounts of substituted Al and Cr (1.6 and 0.7%, on average, respectively).

The properties of α-FeOOH crystallized in the presence of Cr^{3+} ions were investigated for better understanding of the protective role of some metal additions to the weathering steel, during atmospheric corrosion [7,8]. Schwertmann et al. [9] measured the unit-cell parameters for Cr-substituted α-FeOOH samples.

Dos Santos et al. [10] found that up to 10 mol% of gallium can be incorporated into the α-FeOOH structure, and that an increase of gallium substitution reduced crystallite size. Berry et al. [11] prepared Sn-doped α-FeOOH by the hydrothermal method. Mössbauer spectroscopy showed that originally added Sn^{2+} ions were oxidized to Sn^{4+}, whereas Fe^{3+} reduction was not noticed. On the basis of this finding, it was concluded that the charge balance in Sn-doped α-FeOOH was achieved by the formation of cation vacancies. The ^{119}Sn Mössbauer spectra were consistent with octahedrally coordinated tin ions in the α-FeOOH structure.

Al-substituted α-FeOOH is an important constituent of many soils. Al-substitutions influence dissolution and adsorption/desorption properties of α-FeOOH. In a chemical laboratory, Al-substituted α-FeOOH samples were precipitated by adding concentrated KOH solution into the aqueous solution of $Fe(NO_3)_3 + Al(NO_3)_3$ [12] or by adding a solution of aluminate complex into the $Fe(NO_3)_3$ solution [13]. The precipitates thus formed were aged at different temperatures for varying times. Schulze [14] measured the unit-cell parameters of synthetic and Al-substituted α-FeOOH. These measurements showed that the c-dimension was a linear function of Al substitution in the range 0–33 mol% Al, the a-dimension was variable over the same concentration range, whereas the b-dimension slightly deviated from linearity in the range 20–33 mol% Al. Mössbauer spectroscopy found important application in the investigation of Al-doped α-FeOOH [15–19].

In our previous work [20], we reported a novel method for the synthesis of acicular α-FeOOH particles in highly alkaline pH-medium by using tetramethylammonium hydroxide (TMAH) as a precipitating agent for Fe^{3+} ions. The same precipitation method for the synthesis of α-FeOOH has been used in the present work, however, in the presence of Ru-dopant. In this report, we present new results about the influence of Ru-dopant on possible formation of solid solutions, the microstructural properties of the particles, as well as about the overall precipitation process. The samples were investigated by Mössbauer and FT-IR spectroscopies, thermal FE SEM and EDS. Mössbauer spectroscopy is specifically important method in the investigation of iron oxyhydroxides and oxides.

2. Experimental

Analytical reagents, $FeCl_3 \cdot 6H_2O$ and $Ru(NO)(NO_3)_3$, were used. Tetramethylammonium hydroxide solution (25%, w/w, electronic grade 99.9999%) supplied by Alfa Aesar was used. Twice distilled water prepared in our own laboratory was used in all experiments. The experimental conditions for the preparation of samples are given in Table 1. A predetermined volume of the TMAH solution was added to the mixed $FeCl_3 + Ru(NO)(NO_3)_3$ solutions (samples FR1–FR5). Reference sample G was synthesized without $Ru(NO)(NO_3)_3$ component. The suspensions formed were vigorously shaken for approximately 10 min, then heated at 160 °C, using the general-purpose bomb by Parr (model 4744), comprising the vessel and cup made by Teflon. After 2 h of heating, the precipitates were cooled to room temperature (mother liquid pH ~ 13.7) and subsequently washed with twice distilled water using an ultra-speed centrifuge Sorvall RC2-B. After drying, all precipitates were characterized by Mössbauer and FT-IR spectroscopies, thermal FE SEM and EDS. Nominal concentrations of Fe and Ru in the precipitates were confirmed by quantitative EDS analysis.

^{57}Fe Mössbauer spectra were recorded in transmission mode using standard instrumental configuration by WISSEL GmbH (Starnberg, Germany). The ^{57}Co in the rhodium matrix was used as a Mössbauer source. The velocity scale and all the data refer to the metallic α-Fe absorber at RT. Quantitative analysis of the spectra recorded was made using the MOSSWINN program.

FT-IR spectra were recorded at RT using a Perkin-Elmer spectrometer, model 2000. The FT-IR spectrometer was coupled with a personal computer loaded with the IRDM (IR data manager) program to process the recorded spectra. The

Table 1
Experimental conditions for the synthesis of samples G and FR1–FR5

Sample	2 M $FeCl_3$ (ml)	[$FeCl_3$] (M)	0.1 M $Ru(NO)(NO_3)_3$ (ml)	0.01 M $Ru(NO)(NO_3)_3$ (ml)	[$Ru(NO)(NO_3)_3$] (M)	[Ru]/([Ru] + [Fe])	H_2O (ml)	TMAH[a] (ml)
G	2	0.1	–	–	0	0	28	10
FR1	2	0.1	–	4	0.001	0.0099	24	10
FR2	2	0.1	–	8	0.002	0.0196	20	10
FR3	2	0.1	–	12	0.003	0.0291	16	10
FR4	2	0.1	2	–	0.005	0.0476	26	10
FR5	2	0.1	4	–	0.010	0.0909	24	10

[a] TMAH: tetramethylammonium hydroxide (25%, w/w).

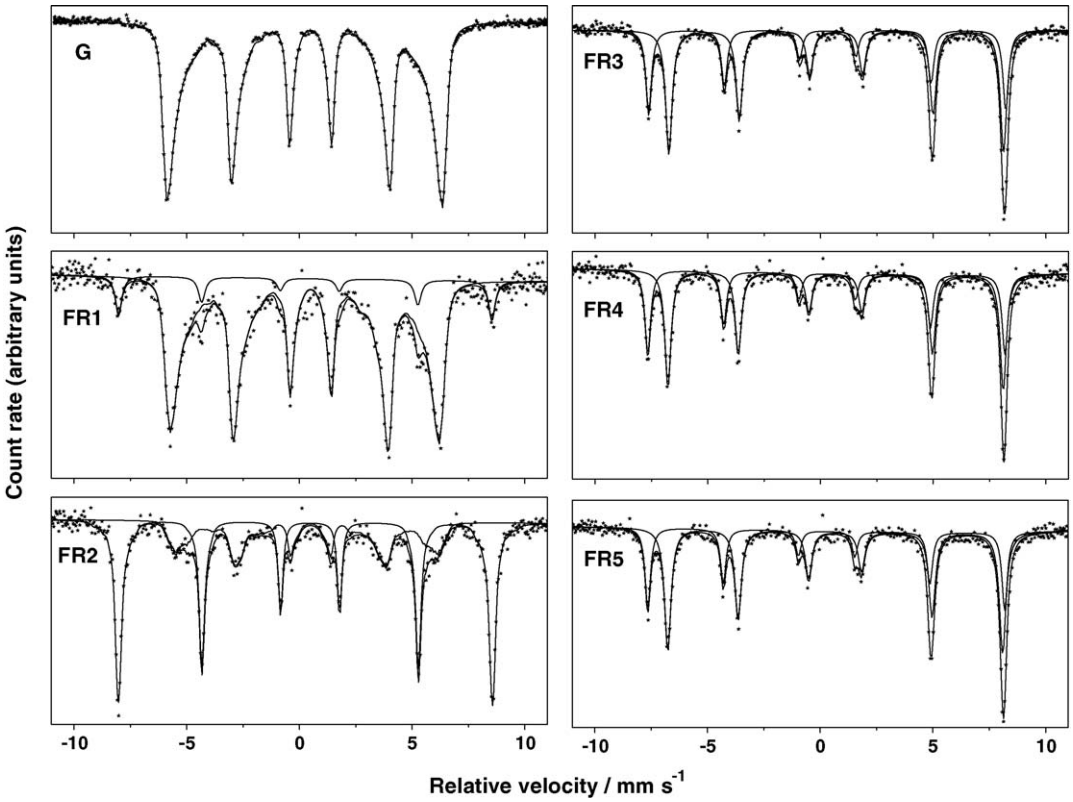

Fig. 1. ^{57}Fe Mössbauer spectra of samples G and FR1–FR5, recorded at RT.

specimens were pressed into small discs using a spectroscopically pure KBr matrix.

JSM-7000F, thermal field emission scanning electron microscope (FE SEM) manufactured by JEOL Ltd., was used. FE SEM was coupled with EDS/INCA 350 (energy dispersive X-ray analyzer) manufactured by Oxford Instruments Ltd.

3. Results and discussion

3.1. ^{57}Fe Mössbauer spectroscopy

The results of Mössbauer spectroscopic measurements are summarized in Figs. 1 and 2 and Table 2. The Mössbauer spectrum of reference α-FeOOH (sample G) shows sextet at RT with broadened spectral lines which deviate from the theoretical intensity ratio 3:2:1:1:2:3. Generally, RT Mössbauer spectrum of undoped α-FeOOH may vary from one paramagnetic doublet up to a well-shaped sextet. α-FeOOH particles smaller than about 15–20 nm show superparamagnetic behavior, whereas the particles smaller than 8 nm remain superparamagnetic down to 77 K. Mössbauer spectrum of sample G, shown in Fig. 1, was fitted taking into account the distribution of hyperfine magnetic fields (HMF) (Fig. 2). The introduction of a small amount of Ru-dopant in the precipitation system caused significant changes as shown with Mössbauer spectra FR1 and FR2. Outer sextet with 51.4 T can be assigned to α-Fe_2O_3. Table 2 shows that in the case of FR1 sample, 9.3% of absorption area corresponded to α-Fe_2O_3, whereas in the case of FR2 sample 64.8% corresponded to α-Fe_2O_3. A decrease of average HMF value of 35.1 T as recorded for sample G to 31.3 T for sample FR2 can be regarded as a

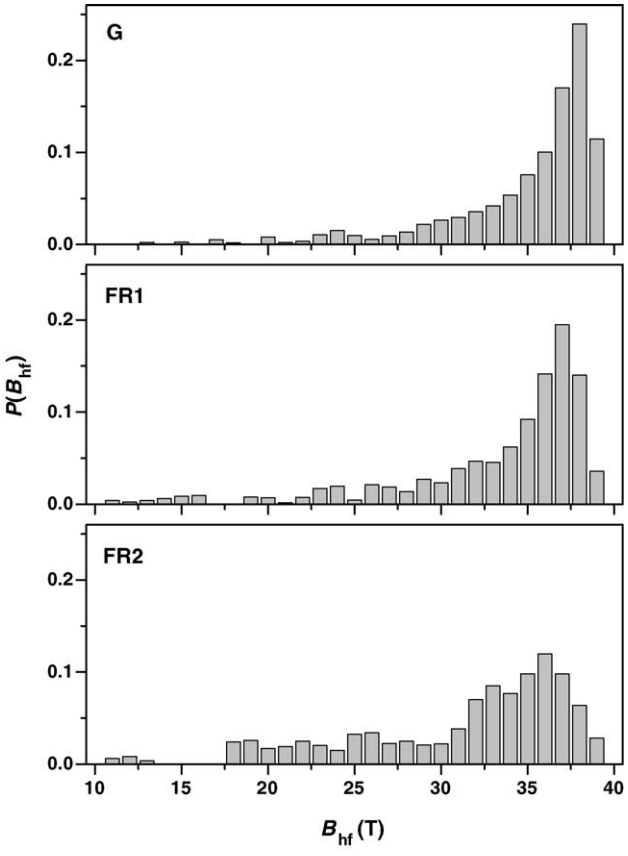

Fig. 2. Distribution of hyperfine magnetic field in α-FeOOH calculated for samples G, FR1 and FR2.

Table 2
^{57}Fe Mössbauer parameters calculated for samples G and FR1–FR5

Sample	Spectral line	δ (mm s^{-1})	E_q (mm s^{-1})	B_{hf} (T)	Γ (mm s^{-1})	Area (%)
G	M	0.37	−0.26	35.1	0.27	100
FR1	M_1	0.37	−0.27	33.4	0.28	90.7
	M_2	0.36	−0.20	51.4	0.35	9.3
FR2	M_1	0.40	−0.19	31.3	0.19	35.2
	M_2	0.37	−0.21	51.4	0.22	64.8
FR3	M_1	0.31	−0.02	49.1	0.31	36.6
	M_2	0.70	0.00	46.0	0.35	63.4
FR4	M_1	0.28	−0.03	49.1	0.31	39.0
	M_2	0.67	0.01	46.1	0.33	61.0
FR5	M_1	0.28	−0.02	49.1	0.29	34.3
	M_2	0.66	0.01	46.1	0.35	65.7

Errors: $\delta = \pm 0.01$ mm s^{-1}, $E_q = \pm 0.01$ mm s^{-1}, $B_{hf} = \pm 0.2$ T. Isomer shift is given relative to α-Fe.

consequence of the formation of a solid solution of ruthenium ions into α-FeOOH. On the other hand, HMF = 51.4 T obtained for α-Fe_2O_3 in samples FR1 and FR2 is close to the value of monolithic α-Fe_2O_3 (HMF = 51.7 T), and for this reason it can be concluded that Ru-dopant did not show a tendency to form the solid solution with α-Fe_2O_3. However, the incorporation of some traces of ruthenium ions into the α-Fe_2O_3 structure cannot be excluded. It is evident that the presence of ruthenium ions caused the formation of α-Fe_2O_3, as well as an increase in the rate of α-Fe_2O_3 crystallization. With further increase of ruthenium concentration up to [Ru]/([Ru] + [Fe]) = 0.0909, stoichiometric Fe_3O_4 was formed as shown in Mössbauer spectra of samples FR3–FR5. Mössbauer parameters calculated are in accordance with the literature data [21].

van Zyl et al. [22] coprecipitated the solution of $ZrOCl_2 + RuCl_2$ salts with concentrated NH_3·aq solution, then the coprecipitate was heated at high temperatures. At lower temperatures, the dissolving of RuO_2 into the ZrO_2 lattice was observed, whereas for a prolonged time of heating at 600 °C the segregation of these two oxides was obtained. In our work, we used $Ru(NO)(NO_3)_3$ solution, because aqueous $RuCl_3$ solution is very susceptible to hydrolysis, oxidation to Ru(IV) and formation of colloidal ruthenium (hydrous) oxide particles. The present work showed for certain only the incorporation of Ru-dopant into the α-FeOOH structure. Crystallization of α-FeOOH was promoted to a certain level in the presence of ruthenium ions and for this reason upon increase of ruthenium concentration the nucleation and crystal growth of α-Fe_2O_3 is favored. In both cases, the starting "amorphous" or ferrihydrite-like precipitate, obtained by TMAH addition into the solution of iron and ruthenium ions, was generator of Fe^{3+} ions for the crystallization of α-FeOOH and α-Fe_2O_3. Initially formed "amorphous" $Fe(OH)_3$ or ferrihydrite-like precipitate was dissolving, and, on the other hand, α-FeOOH and α-Fe_2O_3 reprecipitated. In the absence of ruthenium ions, there was no α-Fe_2O_3 reprecipitation.

With a further increase of an initial concentration of $Ru(NO)^{3+}$ ions, the stoichiometric magnetite (samples FR3–FR5) as a single phase was formed, as documented by Mössbauer spectroscopy. Mössbauer spectroscopy did not give evidence about the incorporation of ruthenium ions into the Fe_3O_4 structure, i.e. the formation of solid solution. The formation of Fe_3O_4 could be explained by the catalytic activity of ruthenium (hydrous) oxide particles. Generally, ruthenium dioxide, ruthenium black and ruthenium supported on various carriers are well-known catalysts. In the present work, we used TMAH as a strong organic alkali, which decomposes at elevated temperatures giving dominantly NH_3, volatile amines and CH_3OH. In the presence of ruthenium catalysts, NH_3 decomposes to N_2 and H_2, whereas CH_3OH decomposes to CO and H_2. In the present experiments, it should be a formation of nascent hydrogen which easily reduces Fe^{3+} to Fe^{2+}, thus creating conditions for the formation of Fe_3O_4 at high pH.

The effects of ruthenium noticed in the present work can be indirectly related with some other works in ruthenium chemistry. Basinska et al. [23] investigated the effect of the carrier on water–gas shift reaction (WGSR) activity of ruthenium catalysts. The formation of Fe_3O_4/γ-Fe_2O_3 by reduction of α-Fe_2O_3 was noticed. Berry et al. [24] used in situ ^{57}Fe Mössbauer spectroscopy to investigate the effects of pretreatment of titania-supported iron-ruthenium and iron-iridium catalysts in hydrogen atmosphere. Musić et al. [25] investigated denitration of simulated highly radioactive liquid waste (HRLW) of several chemical compositions using formic acid as reducing agent. Ruthenium added as $Ru(NO)(NO_3)_3$ or so-called soluble $RuO_2 \cdot xH_2O$ played an important role as catalyst. This reaction was also catalyzed by Rh^{3+} ions, and much less (or not at all) by Pd^{2+} ions. Fe^{3+} was reduced to Fe^{2+}, and then reoxidized to Fe^{3+} with careful addition of concentrated H_2O_2. α-FeOOH and amorphous fraction were the principal phases in the precipitates formed upon oxidation of Fe^{2+} with H_2O_2. Thermal treatment of isolated precipitates caused the solid state transformation of α-FeOOH + amorphous fraction into α-Fe_2O_3. The decreased HMF values in the corresponding Mössbauer spectra were assigned to incorporated metal cations into the α-Fe_2O_3 structure. Musić and Ristić [26] also investigated adsorption of ruthenium on "amorphous" $Fe(OH)_3$, α-Fe_2O_3 and Fe_3O_4. The adsorption of ruthenium increased markedly in the 3–5.5 pH range following the general adsorption behavior of metal cations [27]. At higher pH values, α-Fe_2O_3 showed different behavior with respect to ruthenium adsorption on "amorphous" $Fe(OH)_3$ (coprecipitation) and Fe_3O_4 (adsorption). An abrupt decrease of ruthenium adsorption on α-Fe_2O_3 was noticed for pH higher than ∼7. Fe_3O_4 stabilized ruthenium in lower oxidation states with Fe^{2+}, whereas the formation of negatively charged ruthenate and perruthenate anions was prevented in "amorphous" $Fe(OH)_3$ by the coprecipitation mechanism and similar ionic radii of Fe^{3+} (0.645 Å) and Ru^{4+} (0.62 Å) [28].

3.2. FT-IR spectroscopy

Fig. 3 shows FT-IR spectra of samples G and FR1–FR5. FT-IR spectrum of sample G corresponds to α-FeOOH. At high wave numbers, two intensive and broad bands at 3420 and 3163 cm^{-1} are visible. The IR band at 3420 cm^{-1} can be

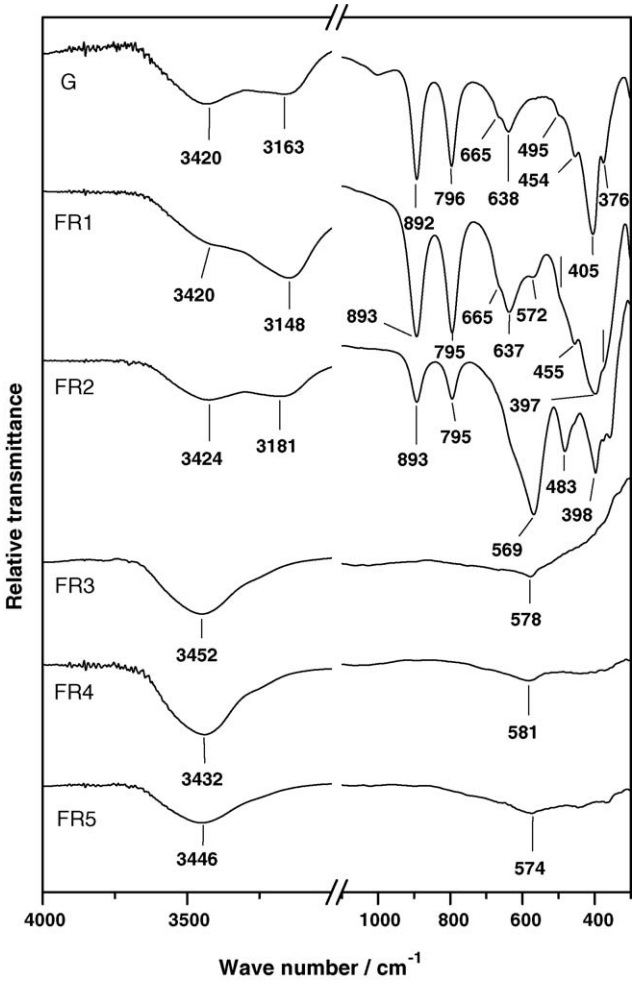

Fig. 3. FT-IR spectra of samples G and FR1–FR5, recorded at RT.

assigned to stretching modes of surface H_2O molecules or to the envelope of the hydrogen bonded surface OH groups [29], whereas the IR band at 3163 cm^{-1} is due to the presence of OH stretching mode in α-FeOOH. Two bands at 892 and 796 cm^{-1} can be assigned to Fe–O–H bending vibrations in α-FeOOH, and these IR bands are generally used for identification of α-FeOOH in phase analysis. Verdonck et al. [30] studied the IR spectrum of α-FeOOH using a normal coordinate analysis method. Experimental and calculated vibrational frequencies for α-FeOOH and deuterated α-FeOOD were compared. In their work, the authors observed that the IR bands at 630, 495 and 270 cm^{-1} were rather insensitive to deuteration, and on the basis of that finding these IR bands were assigned to Fe–O stretching vibrations in α-FeOOH. Cambier [31] gave a similar interpretation of the IR bands noticed for α-FeOOH below 650 cm^{-1}. It was reported that an intense IR band around 630 cm^{-1} is influenced by the shape of the α-FeOOH particles. FT-IR spectrum of α-FeOOH was also discussed by Weckler and Lutz [32].

In the FT-IR spectrum of sample FR1, an additional band at 572 cm^{-1} is visible. FT-IR spectrum of sample FR2 showed an intense IR band at 569 and 483 cm^{-1} which can be assigned to α-Fe_2O_3, whereas the relative intensities of IR bands at 893 and 795 cm^{-1} were decreased. The IR spectrum of α-Fe_2O_3 is influenced by the shape of the particles as published by Iglesias and Serna [33]. α-Fe_2O_3 spheres showed IR bands at 575, 485, 385 and 360 cm^{-1}, whereas α-Fe_2O_3 laths showed IR bands at 650, 525, 440 and 300 cm^{-1}.

FT-IR spectra of samples FR3, FR4 and FR5 are characterized with a broad IR band of weak relative intensity at 578, 581 or 584 cm^{-1}, respectively. On the basis of this IR band, it is not possible to conclude with certainty about the presence of Fe_3O_4, as found by Mössbauer spectroscopy (Section 3.1).

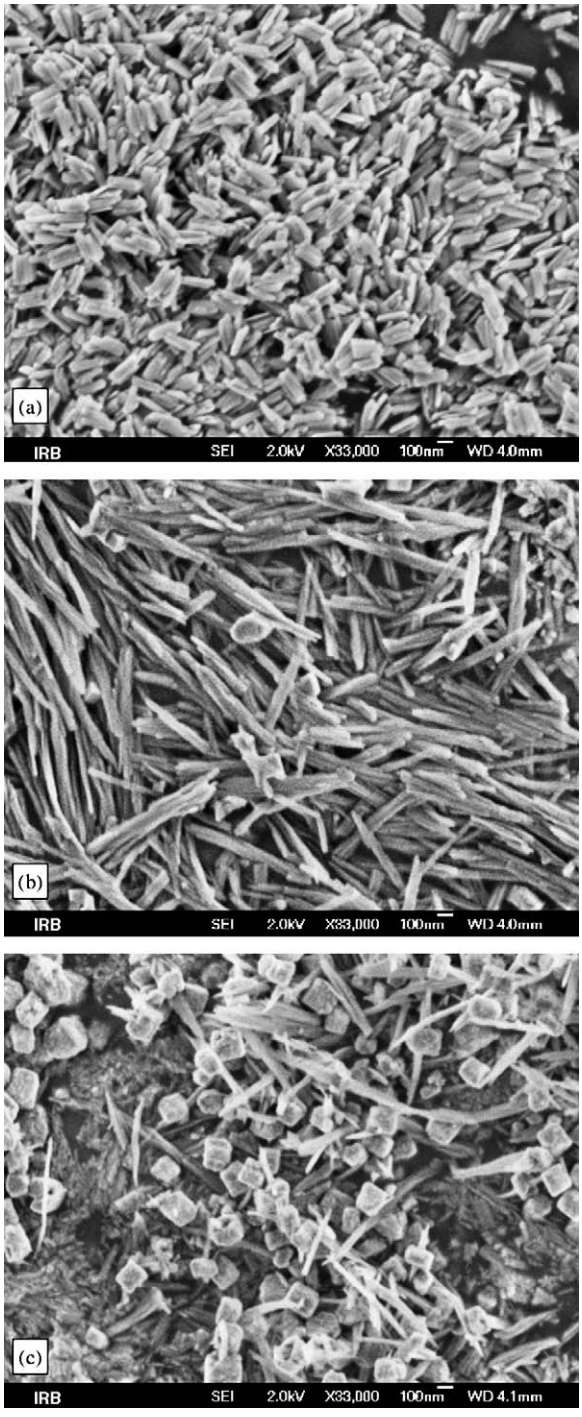

Fig. 4. FE SEM photographs of samples: (a) G, (b) FR1 and (c) FR2 taken at the same optical magnification.

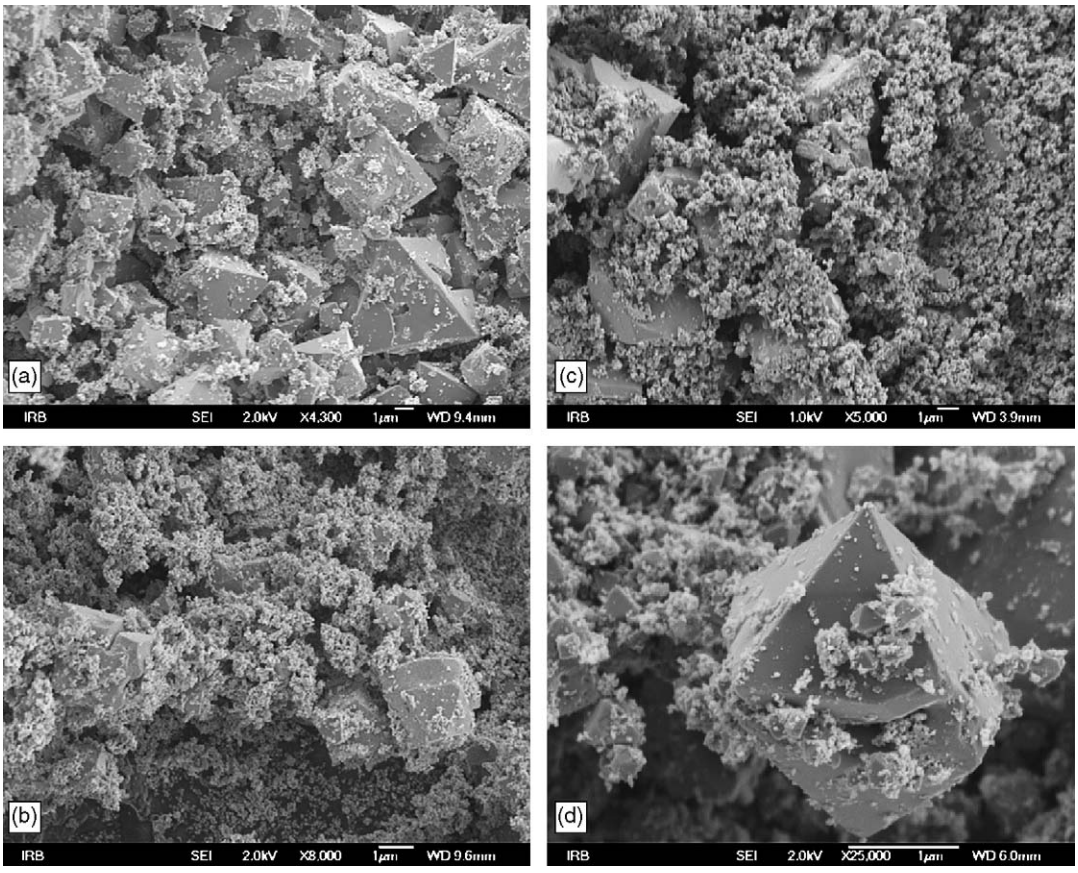

Fig. 5. FE SEM photographs of samples: (a) FR3, (b) FR4, (c) FR5 and (d) FR5 (at a higher optical magnification).

The IR band centered at 3452, 3432 or 3446 cm^{-1} can be interpreted as in the case of previous samples. The origin of this IR band for samples FR3–FR5 may be due to the adsorbed H_2O molecules on Fe_3O_4 surfaces, as well as to the presence of ruthenium (hydrous) oxide particles. Ishii et al. [34] recorded for Fe_3O_4 two characteristic IR bands at 565 and 360 cm^{-1}. These IR bands may be assigned to the $\nu_1(F_{1u})$ and $\nu_2(F_{1u})$ modes, respectively.

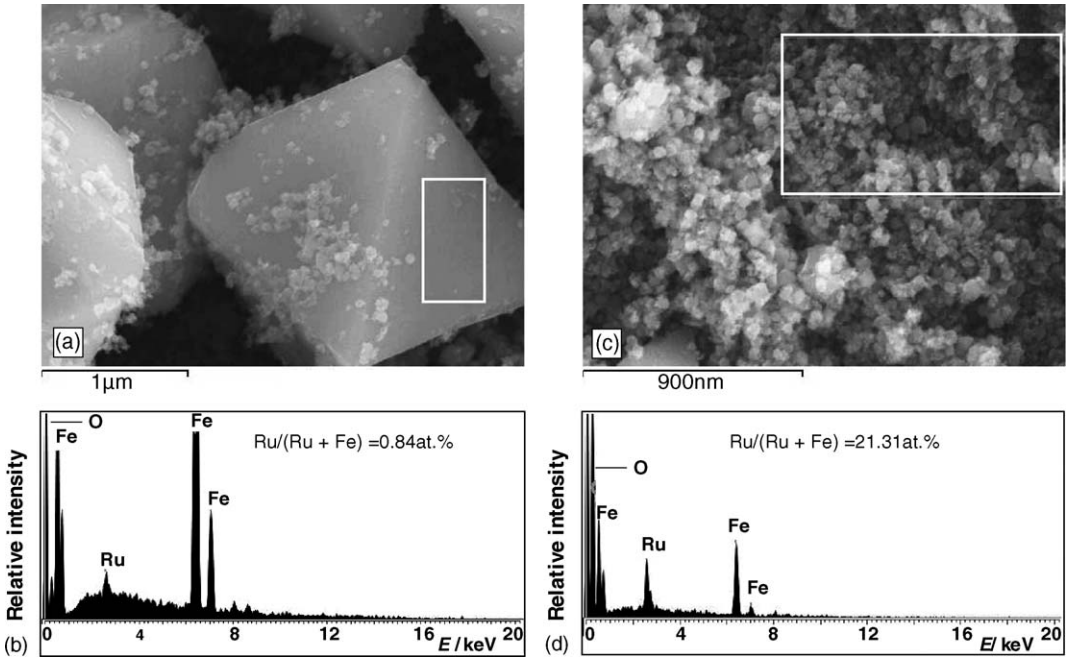

Fig. 6. FE SEM photographs of sample FR3 (a and c) and EDS spectra of selected areas (b and d).

3.3. FE SEM and EDS

Fig. 4 shows FE SEM photographs of samples G, FR1 and FR2 taken at the same magnification. Undoped α-FeOOH contained acicular particles of good uniformity (Fig. 4a). Doping of α-FeOOH with ruthenium ions caused significant elongation of α-FeOOH particles, up to ∼5 times in length, as shown in Fig. 4b. Elongation of α-FeOOH particles with increase of ruthenium concentration was also promoted by the preferential adsorption of ruthenium ions along the *c*-axis. With further incorporation of Ru-dopant in the α-FeOOH structure, the width of α-FeOOH particles was decreased and α-Fe_2O_3 particles were dominant (Fig. 4c) in accordance with Mössbauer spectroscopic results. The locations of IR bands of α-Fe_2O_3 are in accord with the pseudospheric shape of α-Fe_2O_3 particles. Fig. 5 shows big and well-shaped octahedral magnetite particles (crystals) and small particles of ruthenium (hydrous) oxide (sample FR3). A similar size and shape of the particles (crystals) is noticed for samples FR4 and FR5 as shown in Fig. 5b and c. An enlarged detail of one big Fe_3O_4 crystal and small ruthenium (hydrous) oxide particles (sample FR5) is shown in Fig. 5d. These small ruthenium (hydrous) oxide particles, as found by FE SEM, ruled out the formation of ruthenate and perruthenate anions. Fig. 6 shows EDS spectra of selected areas in FE SEM photographs of sample FR3. Microanalysis of one plane of Fe_3O_4 crystal, relatively free from ruthenium (hydrous) oxide particles, showed a small amount of ruthenium (0.84 at%), whereas the microanalysis of the area populated mainly by small particles showed that in this case there is high concentration of ruthenium (21.31 at%). Taking into account these measurements, it can be concluded that Fe_3O_4 particles (crystals) are almost (or totally) free from ruthenium. On the other hand, small ruthenium (hydrous) oxide particles in the range ∼100 nm or less were formed.

4. Conclusions

- Ruthenium ions showed a complex influence on the formation of α-FeOOH, α-Fe_2O_3 and Fe_3O_4 in highly alkaline media. Introduction of small amounts of Ru-dopant in the precipitation system caused a formation of α-Fe_2O_3, besides α-FeOOH which was formed as a single phase in the absence of Ru-dopant. A decrease of HMF from 35.1 T as recorded for α-FeOOH at RT to 31.3 T for sample with [Ru]/([Ru] + [Fe]) = 0.0196 can be assigned to the formation of solid solutions in α-FeOOH. Ru-dopant did not show a tendency to form a solid solution with α-Fe_2O_3.
- Mössbauer spectroscopy showed the formation of stoichiometric Fe_3O_4 between [Ru]/([Ru] + [Fe]) = 0.0291–0.0909. The formation of solid solutions into the Fe_3O_4 with Ru-dopant was not proved. Mössbauer spectroscopy showed a high advantage over FT-IR spectroscopy in the characterization of Fe_3O_4.
- Undoped α-FeOOH contained acicular particles of good uniformity which increased the length up to ∼5 times with increase of the concentration of Ru-dopant. Large octahedral Fe_3O_4 crystals were associated with small particles of ruthenium (hydrous) oxide with size in the range ∼100 nm or less.
- The formation of Fe_3O_4 was suggested to proceed by the catalytic action of ruthenium that created reduction conditions for Fe^{3+} ions and formation of Fe^{2+} in the presence of TMAH at hydrothermal conditions.

References

[1] T. Huynh, A.R. Tong, B. Singh, B.J. Kennedy, Clays Clay Miner. 51 (2003) 397–402.
[2] E.E. Sileo, P.S. Solís, C.O. Paiva-Santos, Powder Diffr. 18 (2003) 50–55.
[3] B. Singh, D.M. Sherman, J.F.W. Mosselmans, R.J. Gilkes, M.A. Wells, Clay Miner. 37 (2002) 639–649.
[4] W. Stiers, U. Schwertmann, Geochim. Cosmochim. Acta 49 (1985) 1909–1911.
[5] R.E. Vandenberghe, A.E. Verbeeck, E. De Grave, W. Stiers, Hyperfine Interact. 29 (1986) 1157–1160.
[6] M.L.M. de Carvalho e Silva, C.S.M. Partiti, J. Enzweiler, S. Petit, S.M. Netto, S.M.B. De Oliveira, Hyperfine Interact. 142 (2002) 559–576.
[7] A.L. Morales, C.A. Barrero, F. Jaramillo, C. Arroyave, J.-M. Greneche, Hyperfine Interact. 148/149 (2003) 135–144.
[8] R. Balasubramanian, D.C. Cook, M. Yamashita, Hyperfine Interact. 139/140 (2002) 167–173.
[9] U. Schwertmann, U. Gasser, H. Sticher, Geochim. Cosmochim. Acta 53 (1989) 1293–1297.
[10] C.A. Dos Santos, A.M.C. Horbe, C.M.O. Barcellos, J.B. Marimon da Cunha, Solid State Commun. 118 (2001) 449–452.
[11] F.J. Berry, Ö. Helgason, A. Bohórquez, J.F. Marco, J. McManus, E.A. Moore, S. Mørup, P.G. Wynn, J. Mater. Chem. 10 (2000) 1643–1648.
[12] D.G. Lewis, U. Schwertmann, Clay Miner. 14 (1979) 115–126.
[13] D.G. Schulze, U. Schwertmann, Clay Miner. 22 (1987) 83–92.
[14] D.G. Schulze, Clays Clay Miner. 32 (1984) 36–44.
[15] E. Murad, U. Schwertmann, Clay Miner. 18 (1983) 301–312.
[16] D.D. Amarasiriwardena, E. De Grave, L.H. Bowen, S.B. Weed, Clays Clay Miner. 34 (1986) 250–256.
[17] L.H. Bowen, E. De Grave, P.M.A. De Bakker, R.E. Vandenberghe, Hyperfine Interact. 54 (1990) 467–472.
[18] E. De Grave, P.M.A. Bakker, L.H. Bowen, R.E. Vandenberghe, Z. Pflanzenernähr, Bodenk 155 (1992) 467–472.
[19] E. De Grave, G.M. Da Costa, L.H. Bowen, C.A. Barrero, R.E. Vandenberghe, Hyperfine Interact. 117 (1998) 245–270.
[20] S. Krehula, S. Popović, S. Musić, Mater. Lett. 54 (2002) 108–113.
[21] E. Murad, J.H. Johnston, Iron oxides and oxyhydroxides, in: G.J. Long (Ed.), Mössbauer Spectroscopy Applied to Inorganic Chemistry, vol. 2, Plenum Publishing Corporation, 1987, pp. 507–582.
[22] W.E. van Zyl, L. Winnubst, T.P. Raming, R. Schmuhl, H. Verweij, J. Mater. Chem. 12 (2002) 708–713.
[23] A. Basinska, L. Kepinski, F. Domka, Appl. Catal. A: Gen. 183 (1999) 143–153.
[24] F.J. Berry, X. Changhai, S. Jobson, J. Chem. Soc. Faraday Trans. 86 (1990) 165–169.
[25] S. Musić, M. Ristić, S. Popović, J. Radioanal. Nucl. Chem. 134 (1989) 353–365.
[26] S. Musić, M. Ristić, J. Radioanal. Nucl. Chem. 109 (1987) 495–506.
[27] S. Musić, M. Ristić, J. Radioanal. Nucl. Chem. 120 (1988) 289–304.
[28] R.D. Shannon, Acta Crystallogr. A 32 (1976) 751–767.
[29] C. Morterra, A. Chiorlno, E. Borello, Mater. Chem. Phys. 10 (1984) 119–138.
[30] L. Verdonck, S. Hoste, F.F. Roelandt, G.P. Van der Kelen, J. Mol. Struct. 79 (1982) 273–279.
[31] P. Cambier, Clay Miner. 21 (1986) 191–200.
[32] B. Weckler, H.D. Lutz, Eur. J. Solid State Inorg. Chem. 35 (1998) 531–544.
[33] J.E. Iglesias, C.J. Serna, Miner. Petrogr. Acta 29A (1985) 363–370.
[34] M. Ishii, M. Nakahira, T. Yamanaka, Solid State Commun. 11 (1972) 209–212.